Toward Optimization of Multi-Pulse, Pulsed Field Magnetization of Bulk High-Temperature Superconductors

Mark D. Ainslie, *Senior Member, IEEE*, Jan Srpcic, Difan Zhou, Hiroyuki Fujishiro, Keita Takahashi, David A. Cardwell, and John H. Durrell

***Abstract*—Pulsed field magnetization (PFM) is the most practical method for magnetizing bulk superconducting materials as trapped field magnets, but the record trapped field achieved by PFM to date is still significantly less than the true trapped field capability of these materials. In this paper, a flexible numerical modeling technique based on the finite element method is used to provide a comprehensive and realistic picture of multi-pulse PFM, which has been shown to be effective in increasing the trapped field/flux over a single pulse. First, the maximum trapped field capability of a representative sample is determined using two types of numerical model simulating field-cooling and zero-field-cooling magnetization. Next, various sets of magnetic field pulses are applied to the bulk to analyze multi-pulse PFM. An increase in the trapped field can be achieved after a second pulse and to do so an increased amplitude of applied field is required to maximize the trapped field fully. The numerical analysis shows that this occurs in subsequent pulses because it is more difficult for the magnetic flux to penetrate the sample and there is a lower temperature rise.**

***Index Terms*—Bulk high-temperature superconductors, finite element method, numerical simulation, pulsed field magnetization, trapped field magnets.**

I. Introduction

BULK superconducting materials can be used as trapped field magnets (TFMs) and magnetic fields greater than 17 T have been achieved in large, single-grain (RE)BCO (where RE = rare earth or Y) bulk high-temperature superconductors [1], [2]. However, developing practical magnetizing techniques is crucial to using them as TFMs in engineering applications, such as rotating machines, magnetic separation and magnetic drug delivery systems [3]–[5].

Manuscript received September 11, 2017; revised December 23, 2017; accepted December 27, 2017. Date of publication January 1, 2018; date of current version January 24, 2018. The work of M. D. Ainslie was supported in part by the Royal Academy of Engineering Research Fellowship and in part by the Engineering and Physical Sciences Research Council Early Career Fellowship EP/P020313/1. The work of H. Fujishiro was supported by JSPS KAKENHI under Grant 15K04646. *(Corresponding author: Mark D. Ainslie.)*

M. D. Ainslie, J. Srpcic, D. Zhou, D. A. Cardwell, and J. H. Durrell are with the Bulk Superconductivity Group, Department of Engineering, University of Cambridge, Cambridge CB2 1PZ, U.K. (e-mail: mark.ainslie@eng.cam.ac.uk).

H. Fujishiro and K. Takahashi are with the Department of Physical Science and Materials Engineering, Faculty of Science and Engineering, Iwate University, Morioka 020-8551, Japan (e-mail: fujishiro@iwate-u.ac.jp).

Color versions of one or more of the figures in this paper are available online at http://ieeexplore.ieee.org.

Digital Object Identifier 10.1109/TASC.2017.2788924

Pulsed field magnetization (PFM) is the most practical method for magnetizing bulk samples as it requires shorter magnetization times (on the order of milliseconds), as well as a more compact and less complicated magnetization fixture. In contrast, the zero field cooling (ZFC) and field cooling (FC) techniques are much slower and require bulky and expensive equipment (usually a large superconducting coil).

The trapped field produced by PFM is generally much smaller than that of ZFC and FC, particularly at lower operating temperatures, because of the large temperature rise, ΔT, associated with the rapid dynamic movement of the magnetic flux in the interior of the superconductor during the pulse [6].

It has been shown that multi-magnetic pulse techniques, such as iteratively magnetizing pulsed-field with reducing amplitude (IMRA) [7] and multi-pulse with step-wise cooling (MPSC) [8], [9], can increase the trapped field/flux. The record trapped field achieved by PFM to date is 5.2 T at 29 K using a modified MPSC (MMPSC) technique [10]; unfortunately, this is still much less than the true trapped field capability of these materials. Numerical models [11]–[13] have been developed that qualitatively reproduce some of the experimentally observed results; here we extend this work to provide a comprehensive and realistic picture of multi-pulse PFM.

In this paper, a 2D axisymmetric finite element method based on the $\boldsymbol{H}$-formulation, previously utilised by the authors for single pulse investigations [14]–[20], is extended to the case of multi-pulse PFM. Firstly, the maximum trapped field capability of a representative bulk sample is estimated using two types of numerical model simulating FC/ZFC magnetization techniques. This establishes a baseline to compare the simulated PFM results. Next, for constant operating temperatures of 77, 65 and 50 K, various sets of magnetic field pulses of amplitude up to 8 T are applied to the bulk. The numerical modeling technique is extremely flexible and can incorporate detailed information on the material properties. Consequently, the results presented will allow the optimization of multi-pulse PFM techniques to enhance the trapped field in bulk high-temperature superconductors.

II. Numerical Simulation Framework

Fig. 1 shows the geometry of the 2D axisymmetric model used in this paper to simulate the solenoid coil magnetization of

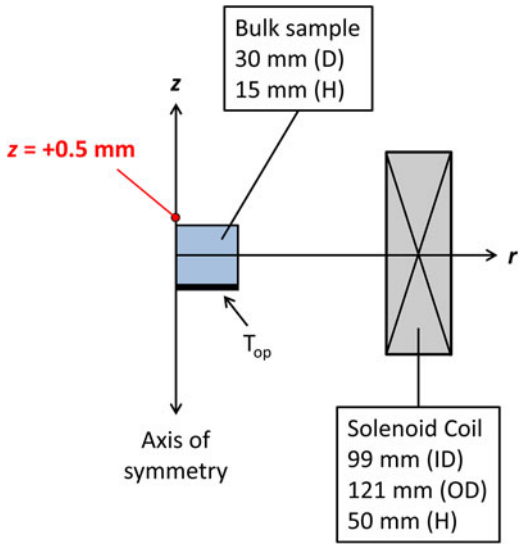

Fig. 1. 2D axisymmetric models for numerical simulation of multi-pulse PFM using a solenoid coil.

a bulk superconductor of diameter (D) 30 mm and thickness (H) 15 mm. Here the sample is cooled from the bottom surface of the bulk with a cold head. The point from which the simulated trapped field is taken is indicated by the red dot, corresponding to the approximate location of a Hall sensor in an actual experimental setup ($z = +0.5$ mm above the centre of the top surface of the bulk).

The electromagnetic properties are simulated using the 2D axisymmetric $\boldsymbol{H}$-formulation, implemented in the commercial software package COMSOL Multiphysics 5.2a. This has been used previously by the authors to simulate bulk high-temperature superconductors under various magnetization conditions [14]–[18], as well as FC magnetization of MgB_2 [19] and iron-pnictide [20] bulks.

The governing equations are derived from Maxwell's equations – namely, Faraday's (1) and Ampere's (2) laws:

$$\nabla \times \boldsymbol{E} + \frac{d\boldsymbol{B}}{dt} = \nabla \times \boldsymbol{E} + \frac{d\left(\mu_0 \mu_r \boldsymbol{H}\right)}{dt} = 0 \tag{1}$$

$$\nabla \times \boldsymbol{H} = \boldsymbol{J} \tag{2}$$

where $\boldsymbol{H} = [H_\mathrm{r},\ H_\mathrm{z}]$ represents the magnetic field components, $\boldsymbol{J} = [J_\phi]$ represents the current density and $\boldsymbol{E} = [E_\phi]$ represents the electric field. μ_0 is the permeability of free space and, for the superconducting and other sub-domains, the relative permeability, μ_r, is simply 1.

The measured in-field critical current density, $J_\mathrm{c}(B, T)$, of a representative bulk high-temperature superconductor (15wt% Ag-containing $GdBa_2Cu_3O_{7-\delta}$) as presented in [17], [18] is used as input data for the model, which is input using a two-variable, direct interpolation [17], [21], [22].

The *E-J* power law ($E\,\alpha\,J^\mathrm{n}$) [23], [24] is used to simulate the non-linear electrical resistivity of the superconductor, where *n* defines the steepness of the transition between the superconducting state and normal state and $n = 20$ as a typical value for HTS materials that is a good approximation of Bean's critical state model [25], [26]. The characteristic voltage criterion $E_0 = 1 \times 10^{-4}$V/m is also assumed.

A pulsed magnetic field, B_app, is generated by a pulsed current flowing in the magnetizing coil (copper coil subdomain). An integral constraint is applied to the copper coil subdomain, as described in [17], using the following I_pulse function (3):

$$I_\mathrm{pulse}\,(t) = N \cdot I_0 \frac{t}{\tau} \exp\left(1 - \frac{t}{\tau}\right) \tag{3}$$

where I_0 is the peak magnitude of the current flowing in each turn of the coil, *N* is the number turns, and $\tau = 15$ ms is the rise time of all pulses in this study, a typical value for standard PFM experiments carried out at Iwate University [17], [27]. In other works, the rise time varies between a few ms to several 10s of ms, depending on the type of magnetizing coil, its inductance/resistance, whether any ferromagnetic materials are used and so on [17], [28], [29]. The magnetizing fixture has the same coil constant, relating B_app, the field at the centre of the magnetizing fixture with the bulk removed, to the applied current, as presented in [17], [18].

Since the temperature of the superconductor can change significantly during PFM [30], the electromagnetic model is coupled with a thermal model, which is based on the following thermal transient equation (4):

$$\rho \cdot C \frac{dT}{dt} = \nabla \cdot (k \nabla T) + Q \tag{4}$$

where *Q* is the heat source calculated from the product of the local electric field and current density, $Q = E_\phi \cdot J_\phi$. The thermal conductivity of the bulk is assumed to be $\kappa_\mathrm{ab} = 20$ W/(m·K) along the *ab*-plane and $\kappa_\mathrm{c} = 4$ W/(m·K) along the *c*-axis [27], [31]. The thermal conductivity of the indium sheet between the bottom surface of the bulk and the cold stage (thickness 0.2 mm) is set to 0.5 W/(m·K) to represent the finite cooling power of the refrigerator and the thermal contact between the bulk and the cold stage, as described in [31].

The temperature rise during the PFM process takes place adiabatically: a large proportion of the heat generated occurs instantaneously, and the low thermal conductivity of the bulk results in thermal diffusion that can be an order of magnitude slower than the magnetic flux diffusion [31]. The measured, temperature-dependent specific heat data for the bulk and indium sheet, as presented in [17], is used. The densities of the bulk and indium sheet are 5900 and 7310 kg/m^3, respectively.

III. Numerical Simulation Results

A. Maximum Trapped Field Capability (FC/ZFC)

The FC/ZFC magnetization techniques allow us to determine the maximum trapped field capability of a bulk sample. Here two types of numerical models are used to estimate the maximum trapped field, which establishes a reliable baseline to compare the simulated PFM results. Table I shows the simulated trapped fields above the centre of the top surface of the bulk ($r = 0$ mm) at a height $z = +0.5$ mm using these two models.

Model #1 (FC) is a stationary model that uses COMSOL's Magnetic Fields (mf) interface in the AC/DC module. The model

TABLE I
FC & ZFC MAGNETIZATION TRAPPED FIELDS

Magnetization	Time	Trapped Field
	77 K	
FC	—	1.544 T
	$t = 0$ min	1.546 T
ZFC [5 T]	$t = 10$ min	1.263 T
	$t = 20$ min	1.223 T
	65 K	
FC	—	3.826 T
	$t = 0$ min	3.827 T
ZFC [10 T]	$t = 10$ min	3.256 T
	$t = 20$ min	3.158 T
	50 K	
FC	—	7.449 T
	$t = 0$ min	7.422 T
ZFC [20 T]	$t = 10$ min	6.577 T
	$t = 20$ min	6.405 T

uses the 'External Current Density' node to assume a current density of $J_c(B)$ flows through the 2D axisymmetric cross-section of the bulk with no flux creep. This is essentially a Bean-like model that takes into account the in-field dependence of J_c and finds a self-consistent solution by solving Ampere's law using the magnetic vector potential $\boldsymbol{A}$ [32].

Model #2 (ZFC) model is similar to that presented in [15], [20], where isothermal conditions are assumed because the magnetization process is slow (uniform applied magnetic field with a ramp rate of 50 mT/s). The finite n value used (20) accounts for flux creep relaxation, resulting in a logarithmic decay of the trapped field after the field is removed. There is good consistency between the FC and ZFC ($t = 0$ min) results, as should be expected [30], and trapped fields of around 80% of this is not an uncommon observation in practical experiments after waiting for flux creep relaxation. The ZFC($t = 20$ min) is used hereafter as a baseline to compare the PFM results. It should be noted that these models do not take into account any mechanical stresses in the bulk that exist during magnetization due to the development of large Lorentz forces, $\boldsymbol{F}_L = \boldsymbol{J} \times \boldsymbol{B}$, for magnetic fields of several tesla or above and can lead to mechanical fracture without appropriate reinforcement [1], [2], [33], [34]. However, it is not difficult to couple such models together and has been the subject of studies elsewhere [35]–[37].

B. Pulsed Field Magnetization – Single Pulse Results

Fig. 2 shows the simulated trapped fields at the centre of the top surface of the bulk ($r = 0$ mm, $z = +0.5$ mm), B_t, after PFM by single pulses of different amplitudes of up to 8 T at operating temperatures of 77, 65 and 50 K using the coupled electromagnetic-thermal model described in Section II. The results are given at $t = 1$ s, as well as $t = 120$ s. The latter results ($t = 120$ s) give ample time for both flux creep relaxation and for the temperature of the bulk to return to the operating temperature, and are used as the input data for subsequent pulses in the multi-pulse models in the following section. The maximum $B_t(t = 120\,\text{s})$ at 77, 65 and 50 K correspond to approximately 85%, 49% and 29% of the ZFC($t = 20$ min) value (see Table I), respectively.

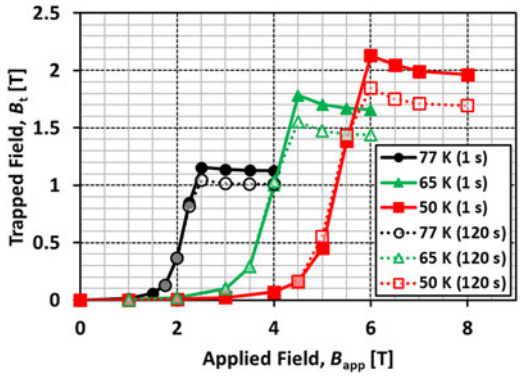

Fig. 2. Numerical simulation results for the trapped magnetic field at the centre of the top surface of the bulk ($r = 0$ mm, $z = +0.5$ mm) after PFM by single pulses of amplitude up to 8 T at operating temperatures of 77, 65 and 50 K. The results are given at $t = 1$ s and 120 s, and the pulse has a rise time, $\tau = 15$ ms.

C. Pulsed Field Magnetization – Multi-Pulse Results – 2nd Pulse

In this section, the influence of subsequent pulses on the trapped field and temperature rise in the bulk are investigated for the multi-pulse PFM technique. The single pulse results from the previous section at $t = 120$ s are used as the input data and a 2nd pulse is applied using (3), but time-shifted such that the pulsed current is $I_{\text{pulse}}(t–t_{2nd})$. Since the magnetic history has an influence on the magnetic flux penetration and temperature rise during subsequent pulses [38], a number of specific cases are investigated here, namely:

1) PM: partially-magnetized (the bulk has an 'M-shaped' [38], [39] trapped field profile across the top surface and little magnetic field is seen at the centre).
2) UM: under-magnetized (the bulk is almost fully magnetized, but does not exhibit a full conical shape).
3) FM: fully-magnetized (the bulk is fully magnetized = full conical shape, and attains the maximum trapped field value for all pulses).
4) OM: over-magnetized (the bulk is fully magnetized, but the trapped field is less due to a larger temperature rise from the higher amplitude of the applied pulse, higher than that of the preceding FM case).

Fig. 3 shows the simulated trapped field profiles across the top surface of the bulk ($z = +0.5$ mm) after PFM, corresponding to the 65 K results at $t = 120$ s shown in Fig. 2 in Section III-B. These are examples of the specific cases above that will be used as input scenarios for the 2nd pulse investigations that follow.

Figs. 4–6 show the simulated trapped fields at the centre of the top surface of the bulk ($r = 0$ mm, $z = +0.5$ mm), B_t, after PFM ($t = 1$ s) by the 2nd pulse at operating temperatures of 77, 65 and 50 K, respectively. For all operating temperatures, the trapped field after the 2nd pulse exhibits two particular characteristics: 1) an increased trapped field, B_t, when the bulk is fully magnetized, which attains a maximum value when the 1st pulse results in full magnetization, and 2) an increased activation field: the applied field, B_{app}, required to maximize the trapped field fully [27]. These observations are more pronounced as the

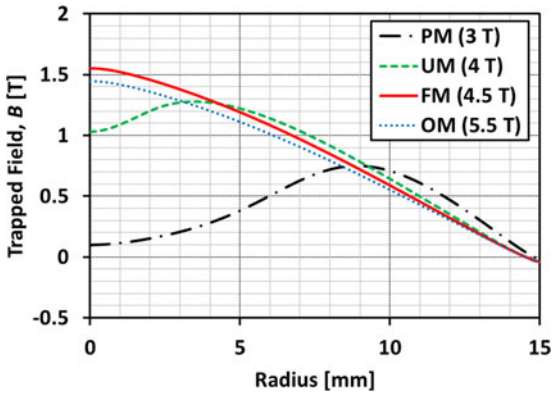

Fig. 3. Numerical simulation results of the trapped magnetic field across the top surface of the bulk ($z = +0.5$ mm) after PFM, corresponding to the 65 K results at $t = 120$ s shown in Fig. 2. These examples show the partially-magnetized (PM, $B_{\rm app} = 3$ T), under-magnetized (UM, $B_{\rm app} = 4$ T), fully-magnetized (FM, $B_{\rm app} = 4.5$ T), and over-magnetized (OM, $B_{\rm app} = 5.5$ T) that are used as input scenarios for the 2nd pulse investigations.

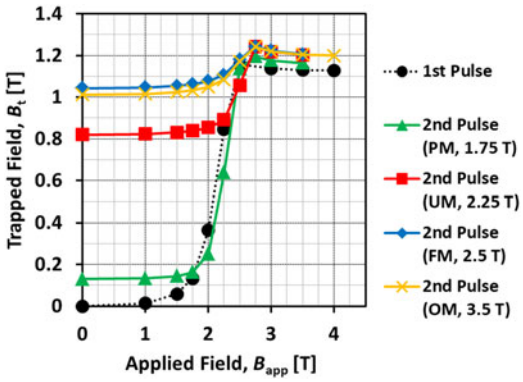

Fig. 4. Numerical simulation results for the trapped magnetic field at the centre of the top surface of the bulk ($r = 0$ mm, $z = +0.5$ mm) after PFM by a 2nd pulse at 77 K ($t = +1$ s from pulse start). Four specific cases of initial magnetization (see Fig. 3) are used as the input data for the 2nd pulse.

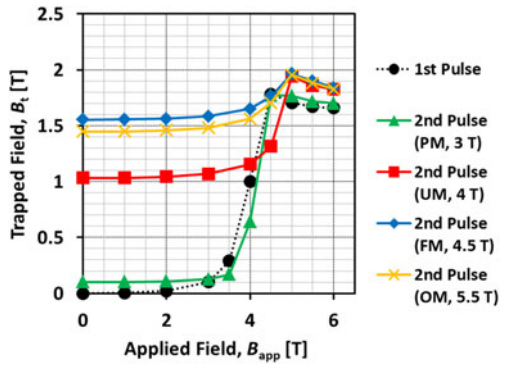

Fig. 5. Numerical simulation results for the trapped magnetic field at the centre of the top surface of the bulk ($r = 0$ mm, $z = +0.5$ mm) after PFM by a 2nd pulse at 65 K ($t = +1$ s from pulse start). Four specific cases of initial magnetization (see Fig. 3) are used as the input data for the 2nd pulse.

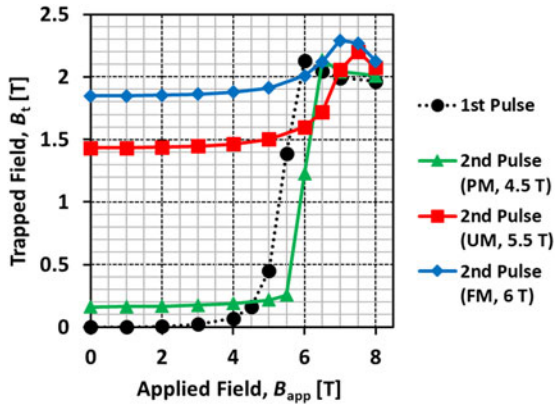

Fig. 6. Numerical simulation results for the trapped magnetic field at the centre of the top surface of the bulk ($r = 0$ mm, $z = +0.5$ mm) after PFM by a 2nd pulse at 50 K ($t = +1$ s from pulse start). Three specific cases of initial magnetization (see Fig. 3) are used as the input data for the 2nd pulse (the OM case is omitted).

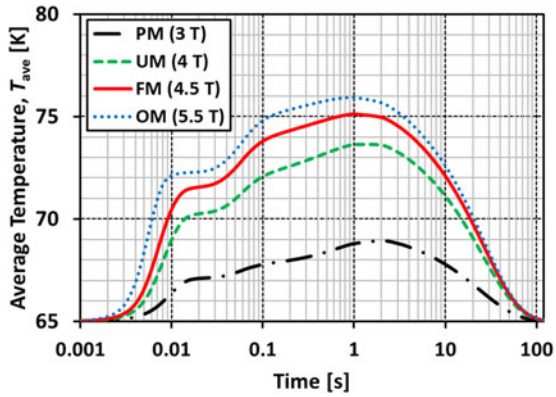

Fig. 7. Numerical simulation results for the average temperature of the bulk, $T_{\rm ave}$, for the four specific cases shown in Fig. 3, corresponding to single pulses at 65 K.

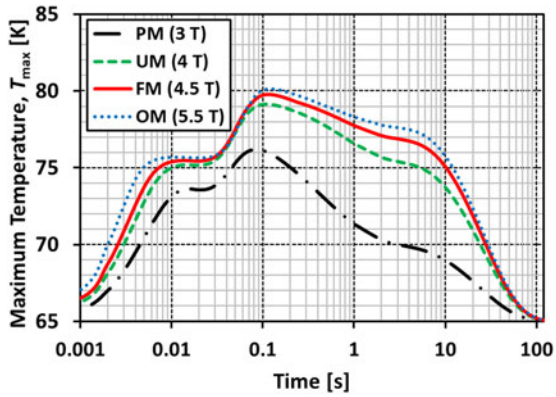

Fig. 8. Numerical simulation results for the maximum temperature of the bulk, $T_{\rm max}$, for the four specific cases shown in Fig. 3, corresponding to single pulses at 65 K.

operating temperature is lowered, and the 2nd pulse is less effective when the bulk is only partially-magnetized by the 1st pulse.

Examination of the numerical results in detail permits it to be deduced that this behaviour occurs because it is more difficult for magnetic flux to penetrate the bulk due to the existing trapped field from the 1st pulse (hence, an increased $B_{\rm app}$ is necessary), which has a corresponding induced supercurrent that flows in the opposite direction. This also results in a lower temperature rise because of the reduced dynamic movement of the magnetic flux within the bulk (hence, $B_{\rm t}$ is higher) [13]. Figs. 7 and 8 shows the simulated average temperature of the bulk, $T_{\rm ave}$, and

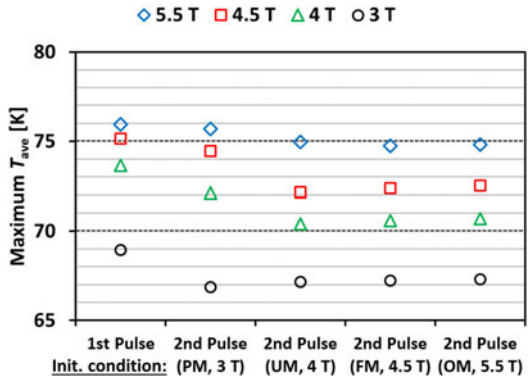

Fig. 9. Numerical simulation results for the maximum average temperature of the bulk, $T_{\mathrm{ave,max}}$, for each of the sets of 2nd pulses, for the four specific cases of initial magnetization (see Fig. 3).

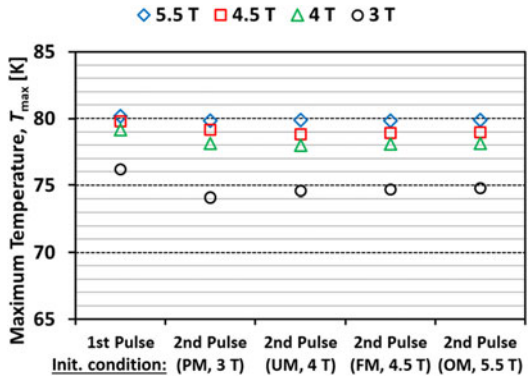

Fig. 10. Numerical simulation results for the maximum temperature of the bulk, T_{max}, for each of the sets of 2nd pulses, for the four specific cases of initial magnetization (see Fig. 3).

maximum temperature, T_{max}, respectively, for the four specific cases shown in Fig. 3, corresponding to single pulses at 65 K. This shows the clear evolution of T_{ave} and T_{max}, corresponding to heating during the rise and fall of the pulse, then thermal diffusion and subsequent cooling, which occurs over a much longer time scale than the magnetic flux diffusion, during the relaxation time to $t = 120$ s. Fig. 9 shows the simulated maximum average temperature, $T_{\mathrm{ave,max}}$, for each of the sets of 2nd pulses, which is compared with $T_{\mathrm{ave,max}}$ for the initial pulses from Fig. 7. In addition, Fig. 10 shows T_{max} for each of the sets of 2nd pulsed, which is also compared with T_{max} for the initial pulses from Fig. 8. There is a similar trend of increasing temperature with increasing amplitude of applied field, as per Figs. 7 and 8, but the temperature rise is lower during the 2nd pulse in all cases for the same amplitude of applied field as the 1st pulse.

Fig. 11 (left) shows the simulated current density distribution during the pulse rise time at $t = 5$ and 10 ms for a single pulse of 4.5 T, corresponding to the FM case in Fig. 3. Also shown (right) is the current density distribution at the same times during a 2nd pulse of 4.5 T when the 4.5 T single pulse results are used as the initial conditions (1st pulse). The induced supercurrent flowing in the opposite direction from the 1st pulse is clearly shown and it is interesting to note that the maximum B_{t} obtained for the single/1st pulse results in a small region near the centre where current flows in the opposite direction to the main magnetizing

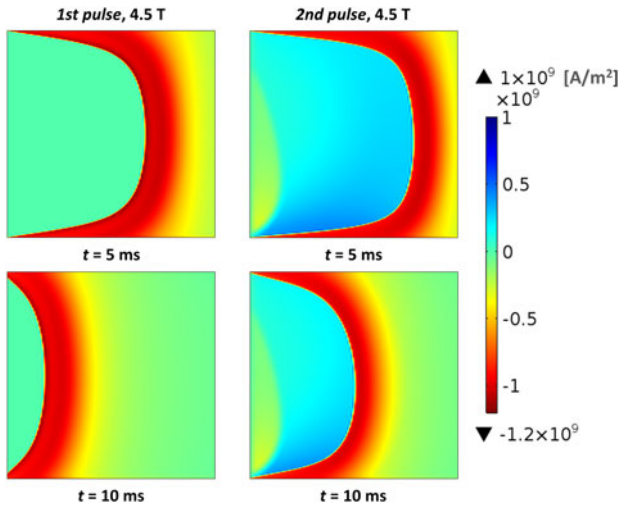

Fig. 11. Numerical simulation results of the current density distribution during the pulse rise time ($t = 5$, 10 ms) for a single pulse of 4.5 T (left; corresponding to the FM case in Fig. 3) and for a 2nd pulse of 4.5 T (right) with results from the single pulse used as the initial conditions (1st pulse).

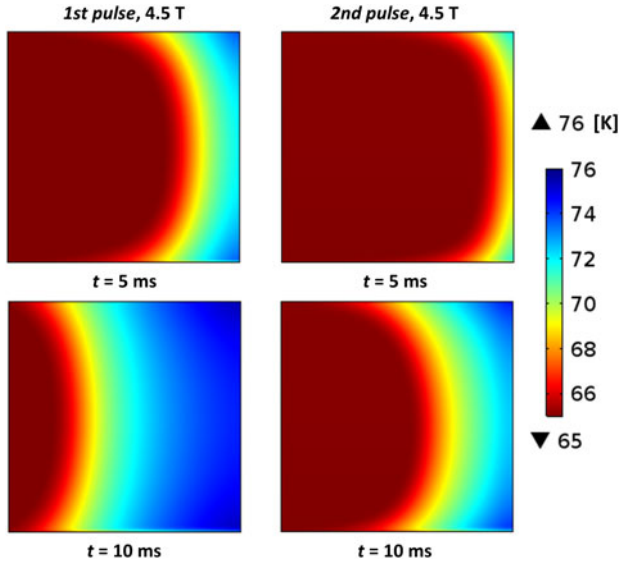

Fig. 12. Numerical simulation results of the temperature distribution during the pulse rise time ($t = 5$, 10 ms) for a single pulse of 4.5 T (left; corresponding to the FM case in Fig. 3) and for a 2nd pulse of 4.5 T (right) with results from the single pulse used as the initial conditions (1st pulse).

current. This was also observed in [38] for the optimum trapped field from stacks of coated conductors. There is some asymmetry in the magnetizing current because the bulk is cooled from the bottom, resulting in a non-uniform temperature distribution. Fig. 12 shows the corresponding temperature distribution for the same cases, which shows clearly the difference in temperature related to changes in the magnetic flux penetration. Fig. 13 shows the simulated magnetic flux penetration across the centre of the bulk during the rising pulse to its peak at 5 ms increments ($\tau = 15$ ms) for a single pulse of 4.5 T (solid lines) and for a 2nd pulse of 4.5 T (dashed lines) with results from the 4.5 T single pulse used as the initial conditions (1st pulse). The magnetic field profile within the bulk is consistent with the current density in

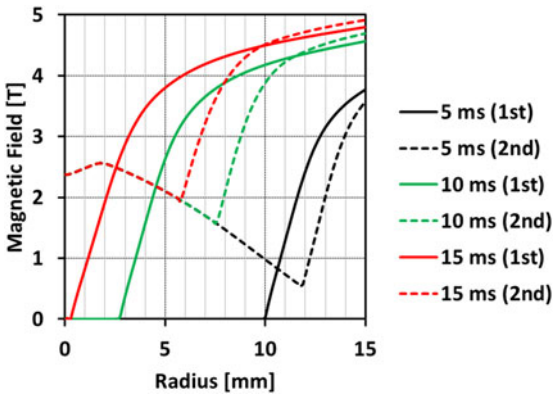

Fig. 13. Numerical simulation results for the magnetic flux penetration across the centre of the bulk during the rising pulse to its peak (5 ms increments; $\tau = 15$ ms) for a single pulse of 4.5 T (solid lines) and for a 2nd pulse of 4.5 T (dashed lines) with results from the single pulse used as the initial conditions (1st pulse).

Fig. 11 and it is clear that it is more difficult for the magnetic flux to penetrate the bulk during the 2nd pulse. Hence, an increased B_{app} is required to fully magnetize the bulk for the 2nd pulse.

These observations have important implications for the determination of the optimum set of pulses that results in the maximum trapped field at a particular operating temperature. It has been previously shown experimentally [29], [39] that an initially partially-magnetized bulk (with an 'M-shaped' trapped field profile) can result in high trapped fields; this is not observed within this numerical simulation framework. This phenomenon may be strongly related to flux jumps during the pulse rise time that can assist the PFM process [18], [28], [29], [40], [41], which also are not observed within this framework. This suggests that some techniques, such as the iteratively magnetizing pulsed-field method with reducing amplitude (IMRA) [7], may be not be as effective without assistive flux jumps.

In the Appendix, Figs. 14–16 show the results for B_{t} for a 3rd pulse for operating temperatures of 77, 65 and 50 K, respectively. Similar results are found for the 3rd pulse as for the 2nd pulses; however, the increase in B_{t} is marginal, suggesting saturation has been reached.

IV. Conclusion

In this paper, a 2D axisymmetric finite element method based on the $\boldsymbol{H}$-formulation is extended to investigate the optimization of multi-pulse PFM techniques. An increase in the trapped field can be achieved after a 2nd pulse and this exhibits two particular characteristics, which are more pronounced at lower operating temperatures: 1) an increased trapped field, B_{t}, when the bulk is fully magnetized, which attains a maximum value when the 1st pulse results in full magnetization, and 2) an increased applied field to fully magnetize the sample. The numerical analysis shows that this occurs because it is more difficult for the magnetic flux to penetrate the sample and there is a lower temperature rise during the 2nd pulse. A partially-magnetized bulk (with an 'M-shaped' trapped field profile) may only be useful for pre-magnetization in the case that flux jumps occur during (and assist) the PFM process.

Acknowledgment

Additional data related to this publication are available at the University of Cambridge data repository (https://doi.org/10.17863/CAM.13608).

Appendix
Pulsed Field Magnetization – Multi-Pulse Results – 3rd Pulse

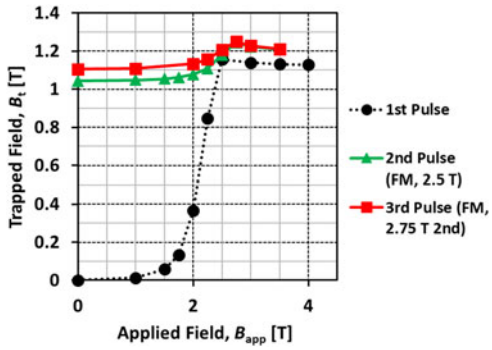

Fig. 14. Numerical simulation results for the trapped magnetic field at the centre of the top surface of the bulk ($r = 0$ mm, $z = +0.5$ mm) after PFM by a 3rd pulse at 77 K ($t = +1$ s from pulse start). The initial conditions for the 2nd and 3rd pulses correspond to the FM case for the preceding pulse (1st = 2.5 T, 2nd = 2.75 T).

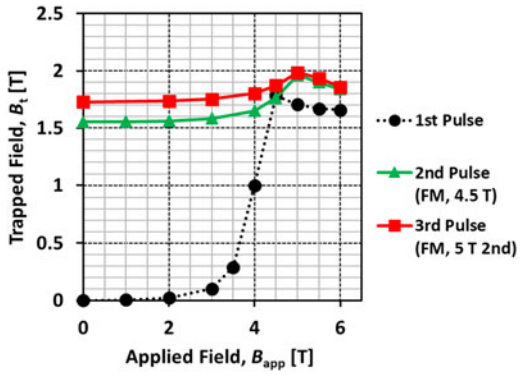

Fig. 15. Numerical simulation results for the trapped magnetic field at the centre of the top surface of the bulk ($r = 0$ mm, $z = +0.5$ mm) after PFM by a 3rd pulse at 65 K ($t = +1$ s from pulse start). The initial conditions for the 2nd and 3rd pulses correspond to the FM case for the preceding pulse (1st = 4.5 T, 2nd = 5 T).

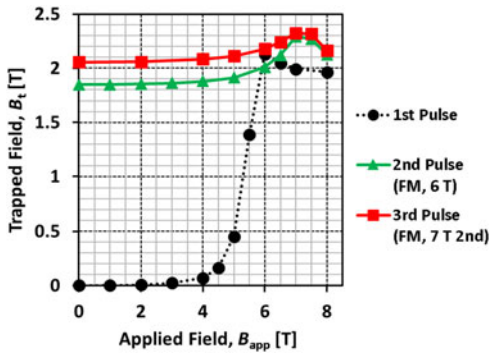

Fig. 16. Numerical simulation results for the trapped magnetic field at the centre of the top surface of the bulk ($r = 0$ mm, $z = +0.5$ mm) after PFM by a 3rd pulse at 50 K ($t = +1$ s from pulse start). The initial conditions for the 2nd and 3rd pulses correspond to the FM case for the preceding pulse (1st = 6 T, 2nd = 7 T).

REFERENCES

[1] M. Tomita and M. Murakami, "High-temperature superconductor bulk magnets that can trap magnetic fields of over 17 tesla at 29 K," *Nature*, vol. 421, pp. 517–520, Jan. 2003.

[2] J. H. Durrell *et al.*, "A trapped field of 17.6 T in melt-processed, bulk Gd-Ba-Cu-O reinforced with shrink-fit steel," *Supercond. Sci. Technol.*, vol. 27, no. 8, 2014, Art. no. 082001.

[3] J. Hull and M. Murakami, "Applications of bulk high-temperature superconductors," *Proc. IEEE*, vol. 92, no. 10, pp. 1705–1718, Oct. 2004.

[4] M. Murakami, "Processing and applications of bulk RE-Ba-Cu-O superconductors," *Int. J. Appl. Ceram. Technol.*, vol. 4, no. 3, pp. 225–241, 2007.

[5] B. Li *et al.*, "Materials process and applications of single grain (RE)-Ba-Cu-O bulk high-temperature superconductors," *Phys. C*, vol. 482, pp. 50–57, 2012.

[6] H. Fujishiro *et al.*, "Pulsed field magnetization of GdBaCuO bulk with stronger pinning characteristics," *IEEE Trans. Appl. Supercond.*, vol. 19, no. 3, pp. 3545–3548, Jun. 2009.

[7] U. Mizutani *et al.*, "Pulsed-field magnetization applied to high-Tc superconductors," *Appl. Supercond.*, vol. 6, nos. 2–5, pp. 235–246, 1998.

[8] M. Sander, U. Sutter, R. Koch, and M. Klaser, "Pulsed magnetization of HTS bulk parts at $T > 77$ K," *Supercond. Sci. Technol.*, vol. 13, pp. 841–845, 2000.

[9] H. Kamijo and H. Fujimoto, "Repeated pulsed-field magnetization with temperature control in a high-T_c bulk superconductor," *IEEE Trans. Appl. Supercond.*, vol. 11, no. 1, pp. 1816–1819, Mar. 2001.

[10] H. Fujishiro *et al.*, "Higher trapped field over 5 T on HTSC bulk by modified pulse field magnetizing," *Phys. C*, vol. 445, pp. 334–338, 2006.

[11] K. Kajikawa *et al.*, "Finite element analysis of pulsed field magnetization process in cylindrical bulk superconductor," *Phys. C*, vol. 468, pp. 1494–1497, 2008.

[12] H. Fujishiro, T. Naito, and D. Furuta, "Analysis of temperature and magnetic field distribution in superconducting bulk during pulsed field magnetization," *IEEE Trans. Appl. Supercond.*, vol. 21, no. 3, pp. 2723–2726, Jun. 2011.

[13] H. Fujishiro, T. Naito, and M. Oyama, "Simulation of flux dynamics in a superconducting bulk magnetized by multi-pulse technique," *Phys. C*, vol. 471, pp. 889–892, 2011.

[14] J. Zou, M. D. Ainslie, D. Hu, and D. A. Cardwell, "Influence of time-varying external magnetic fields on trapped fields in bulk superconductors," *IEEE Trans. Appl. Supercond.*, vol. 25, no. 3, Jun. 2015, Art. no. 4900505.

[15] M. P. Philippe *et al.*, "Influence of soft ferromagnetic sections on the magnetic flux density profile of a large grain, bulk Y-Ba-Cu-O superconductor," *Supercond. Sci. Technol.*, vol. 28, no. 9, 2015, Art. no. 095008.

[16] J. Zou, M. D. Ainslie, D. Hu, and D. A. Cardwell, "Mitigation of demagnetization of bulk superconductors by time-varying external magnetic fields," *IEEE Trans. Appl. Supercond.*, vol. 26, no. 4, Jun. 2016, Art. no. 8200605.

[17] M. D. Ainslie *et al.*, "Enhanced trapped field performance of bulk high-temperature superconductors using split coil, pulsed field magnetization with an iron yoke," *Supercond. Sci. Technol.*, vol. 29, no. 7, 2016, Art. no. 074003.

[18] M. D. Ainslie *et al.*, "Flux jump-assisted pulsed field magnetization of high-Jc bulk high-temperature superconductors," *Supercond. Sci. Technol.*, vol. 29, no. 12, 2016, Art. no. 124004.

[19] J. Zou *et al.*, "Numerical modeling and comparison of MgB2 bulks fabricated by HIP and infiltration growth," *Supercond. Sci. Technol.*, vol. 28, no. 7, 2015, Art. no. 075009.

[20] M. D. Ainslie *et al.*, "Numerical modeling of iron-pnictide bulk superconductor magnetization," *Supercond. Sci. Technol.*, vol. 30, no. 10, 2017, Art. no. 105009.

[21] D. Hu *et al.*, "DC characterization and 3D modeling of a triangular, epoxy-impregnated high temperature superconducting coil," *Supercond. Sci. Technol.*, vol. 28, no. 6, 2015, Art. no. 065011.

[22] D. Hu *et al.*, "Modeling and comparison of in-field critical current density anisotropy in high-temperature superconducting (HTS) coated conductors," *IEEE Trans. Appl. Supercond.*, vol. 26, no. 3, Apr. 2016, Art. no. 6600906.

[23] C. J. G. Plummer and J. E. Evetts, "Dependence of the shape of the resistive transition on composite inhomogeneity in multifilamentary wires," *IEEE Trans. Magn.*, vol. MAG-23, no. 2, pp. 1179–1182, Mar. 1987.

[24] J. Rhyner, "Magnetic properties and AC-losses of superconductors with power law current-voltage characteristics," *Phys. C*, vol. 212, nos. 3/4, pp. 292–300, Jul. 1993.

[25] F. Grilli *et al.*, "Finite-element method modeling of superconductors: From 2-D to 3-D," *IEEE Trans. Appl. Supercond.*, vol. 15, no. 1, pp. 17–25, Mar. 2005.

[26] S. Stavrev *et al.*, "Comparison of numerical models for modeling of superconductors," *IEEE Trans. Magn.*, vol. 38, no. 2, pp. 849–852, Mar. 2002.

[27] M. D. Ainslie *et al.*, "Modeling and comparison of trapped field in (RE)BCO bulk superconductors for activation using pulsed field magnetization," *Supercond. Sci. Technol.*, vol. 27, no. 6, 2014, Art. no. 065008.

[28] R. Weinstein *et al.*, "Observation of a bean model limit — A large decrease in required activation field for TFMs," *IEEE Trans. Appl. Supercond.*, vol. 25, no. 3, Jun. 2015, Art. no. 6601106.

[29] D. Zhou *et al.*, "A portable magnetic field of >3 T generated by the flux jump assisted, pulsed field magnetization of bulk superconductors," *Appl. Phys. Lett.*, vol. 110, 2017, Art. no. 062601.

[30] M. D. Ainslie and H. Fujishiro, "Modeling of bulk superconductor magnetization," *Supercond. Sci. Technol.*, vol. 28, no. 5, 2015, Art. no. 053002.

[31] H. Fujishiro and T. Naito, "Simulation of temperature and magnetic field distribution in superconducting bulk during pulsed field magnetization," *Supercond. Sci. Technol.*, vol. 23, no. 10, 2010, Art. no. 105021.

[32] V. M. R. Zermeno *et al.*, "Estimation of maximum possible trapped field in superconducting permanent magnets in 2D and 3D," arXiv:1606.01817, Jun. 2016.

[33] Y. Ren *et al.*, "Damage caused by magnetic pressure at high trapped field in quasi-permanent magnets composed of melt-textured Y-Ba-Cu-O superconductor," *Phys. C*, vol. 251, nos. 1/2, pp. 15–26, 1995.

[34] G. Fuchs *et al.*, "Trapped magnetic fields larger than 14 T in bulk YBa2Cu3O7-x," *Appl. Phys. Lett.*, vol. 76, no. 15, pp. 2107–2109, Apr. 2000.

[35] H. Mochizuki *et al.*, "Trapped field characteristics and fracture behavior of REBaCuO bulk ring during pulsed field magnetization," *IEEE Trans. Appl. Supercond.*, vol. 26, no. 4, Jun. 2016, Art. no. 6800205.

[36] H. Fujishiro *et al.*, "Simulation studies of mechanical stresses in REBaCuO superconducting ring bulks with infinite and finite height reinforced by metal ring during field-cooled magnetization," *Supercond. Sci. Technol.*, vol. 30, no. 8, 2017, Art. no. 085008.

[37] K. Takahashi *et al.*, "Fracture behavior analysis of EuBaCuO superconducting ring bulk reinforced by a stainless steel ring during field-cooled magnetization," *Supercond. Sci. Technol.*, vol. 30, no. 11, 2017, Art. no. 115006.

[38] S. Zou *et al.*, "Simulation and experiments of stacks of high temperature superconducting coated conductors magnetized by pulsed field magnetization with multi-pulse technique," *Supercond. Sci. Technol.*, vol. 30, no. 1, 2017, Art. no. 014010.

[39] H. Fujishiro *et al.*, "Importance of initial "M-shaped" trapped field profile in a two-stage pulse field magnetization (MMPSC) method," *Physica C*, vol. 463–465, pp. 394–397, 2007.

[40] R. Weinstein *et al.*, "A significant advantage for trapped field magnet applications—A failure of the critical state model," *Appl. Phys. Lett.*, vol. 107, 2015, Art. no. 152601.

[41] R. Weinstein *et al.*, "Anomalous results observed in magnetization of bulk high temperature superconductors—A windfall for applications," *J. Appl. Phys.*, vol. 119, 2016, Art. no. 133906.